Electrocatalytic Activity of Electropolymerized Meldola's Blue toward Oxidation of Dopamine

Electrocatalytic Activity of Electropolymerized Meldola's blue toward Oxidation of Dopamine

Takahiro YAMAGUCHI*, Teruhisa KOMURA, Sayomi HAYASHI, Manabu ASANO,
Guang Yao NIU, Kohshin TAKAHASHI

Division of Material Sciences, Graduate School of Natural Science and Technology,
Kanazawa University (Kakumamachi, Kanazawa, 920-1192, Japan)

To understand the kinetics of charge transfer from chemically modified electrodes to solution species, the authors have investigated the influence of poly(Meldola's blue) on the kinetic parameters of dopamine oxidation by rotating disc electrode voltammetry. The polymer film fixed on electrode surfaces raised the dopamine peak current by a factor of 10 in a 0.1 mM solution; this electrocatalytic effect enables one to detect dopamine at concentrations of the order of 5 μM. The polymer film increased the standard heterogeneous rate constant of dopamine oxidation more than 10-fold and favored a two-electron transfer step, thus raising the dependence of the kinetic current on the electrode potential. These effects were independent of electron self-exchange between redox-active sites in the film. They arose from the incorporation of dopamine with the polymer. This binding interaction decreased with protonation of the polymer, because of electrostatic repulsion between the positively charged species.

Keywords: Chemically modified electrode, Electrocatalytic oxidation, Poly(Meldola's blue), Dopamine, Rotating disc electrode

1. Introduction

Dopamine (3,4-dihydroxyphenethylamine, DA) is a catechol-based neurotransmitter which plays an important role in the mammalian central nervous system. Because DA is rather irreversibly oxidized at metal electrodes, its redox reaction requires a high overpotential. In addition, DA is present at a very low concentration of 0.01–1 μM in the extra-cellular fluid of the central nervous system and has an oxidation potential close to that of ascorbic acid coexisting at a higher concentration[1–4]. Appropriate electrocatalysts are hence necessary for electrochemical detection of DA[5–8]. A number of chemically modified electrodes have been proposed for the determination of this compound; metal electrodes coated with thin films such as metal(II)hexacyanoferrate[9–11], metal phthalocyanines[12,13], and polymers[14–17]. Several workers have reported sensitive or selective voltammetric monitoring of DA[1, 8–20]. Miller and Zhou[21] prepared a composite poly(N-methylpyrrole)-polystyrenesulfonate film to incorporate cationic DA into the reduced polymer. Piro and others[22] have recently developed a new cation-exchanging polymer, poly(5-amino-1,4-naphtoquinone), which can uptake DA up to 100 nmol cm^{-2} in a 300 nm thick film. The DA incorporated was released by applying the oxidative potential to the redox-active polymer. Electrocontrolled release of bio-related materials by polymer-modified electrodes plays a crucial role in delivering drugs at a constant rate to a precise site.

Azines (phenazines, phenothiazines, and phenoxazines) undergo a reversible two-electron, one-proton reduction to yield the corresponding 10-hydro-azine forms; thus these dyes have been often

used as redox indicators and mediators in the field of biotechnological analysis[23–27]. In addition, most of the amino group-substituted azines are irreversibly oxidized to their respective radical cations in aqueous media and have yielded polymeric films on electrode surfaces[27–29], though showing a low current efficiency. Having redox-active properties like those of the corresponding monomers, the electropolymerized azines have attracted a growing interest because of their analytical application[23, 30–33]. Their current-enhancing effects on the hydrogenation-dehydrogenation of myoglobin[34], hemoglobin[34], and NADH[28, 35, 36] prompted us to examine the electrocatalytic activity of polyazines against oxidation of DA.

Voltammetric detection of solution species and electrocatalytic efficiency at polymer-modified electrodes depend primarily on how greatly a surface-immobilized polymer enhances the rate of the redox reaction of a target. Hence, the following subjects need to be investigated: (1) the kinetics of oxidation-reduction of the polymer and (2) its catalytic activity toward the target redox reaction. To understand the mediating properties of polyazines, one requires to examine the rate of coupled electron and proton transport in the electroactive nitrogen-including polymers, because the kinetics of their redox reactions depend on both the reduction and protonation levels. The preceding paper[37] demonstrates that the diffusion coefficient of charge carriers in a polyazine film increases with decreasing solution pH. This change results from electron hopping accompanied by proton transfer. On the other hand, limited data on electron exchange between the catalytic center and solution substrate have hampered a thorough understanding of the selective electrocatalysis due to polyazines.

This paper describes the influence of poly(Meldola's blue) (PMD) films on the kinetic parameters of DA electrooxidation and ascribes the enhanced oxidation rate to the incorporation of DA into the polymer, which arises from their binding interaction.

2. Experimental

Meldola's blue MD^+ (Structure 1), methylene blue, and DA hydrochloride were obtained from Kanto Kagaku Co., and used as received. Sodium sulfate (Wako Chemicals, purity 99.9%) was recrystallized from doubly distilled water and then used as a supporting electrolyte. Thin films of PMD were electrolytically deposited on glassy carbon (GC) of 0.071 cm^2 area by the same method as that used for poly(methylene blue) [37]. The potential of the working electrode was repetitively cycled between -0.4 and 1.6 V (versus Ag/AgCl) at a scan rate of 100 mV s^{-1} in a 1 mM MD^+ solution (pH 8) containing 0.2 M Na_2SO_4. Sample solution contained 20 mM buffer salts, either acetate(pH 4−6), phosphate(pH 6−8) depending on the required pH.

The surface coverage Θ of the resulting polymer, the surface concentration of a two-electron reaction site, was calculated from the voltammetric charge (Q) consumed in reducing the entire polymer at a scan rate of 5 mV s^{-1} in a pure supporting electrolyte solution (pH 4–5):

$$\Theta = Q/2FS \quad (1)$$

where F is the Faraday constant and S is the electrode area. The polymer film was too thin (less than 50 nm) to estimate the film thickness by scanning electron microscopy. The thickness of PMD films given below was calculated from the Θ versus thickness plot measured for poly(methylene blue)[37], assuming that the two polymers are equal in the concentration of electroactive sites. The attenuated total reflection (ATR) infrared spectra of PMD films deposited on electrodes were recorded on a Horiba FT-710 IR spectrophotometer. In situ visible absorption spectrum of the polymer was measured at its different reduction levels with a 10 mm path-length quartz cell containing a polymer-coated indium tin oxide electrode, a platinum wire, and an Ag/AgCl reference electrode.

All the electrochemical experiments were carried out at a temperature of 20 ± 5 ºC under a nitrogen atmosphere with a conventional three-electrode glass cell enclosed in a grounded Faraday cage. A 3 mm diameter GC rod mounted with epoxy resin into a glass tube was used as a working electrode, a platinum gauze of 20 cm^2 area as a counter electrode, and an Ag|AgCl|3.4 M KCl electrode as the reference electrode. The working electrode was polished with aqueous slurries of alumina (down to a grain size of 0.05 μm) and then sonicated in purified water for 5 min. Cyclic voltammetry, differential pulse voltammetry, and potential step chronocoulometry were performed by using a Hokuto Denko HZ-3000 electrochemical system consisting of a FMV Desk Power CIX 407c personal computer, a HAG-1510m potentiostat, and a BJC-F 200 printer. A Hokuto Denko rotating disk electrode system with a glassy carbon electrode (diameter 0.5 cm) was used in the rotating disk electrode experiment.

3. Results and discussion

3.1. Redox properties of PMD

When oxidized at 1.5 to 1.6 V in an aqueous solution buffered at pH 8, the cationic dye MD^+ yielded an electroactive polymer film on GC. Fig. 1 exhibits the cyclic voltammogram of the chemically modified electrode, measured in a 0.2 M H_2SO_4 solution. The electropolymerized dye revealed a pair of redox waves at a half-wave potential $E_{1/2}$ of 0.18 V, which was 0.05 V more negative than the $E_{1/2}$ of the

monomeric dye held in solution. The inset in Fig.1 shows the cathodic peak current I_{pc} plotted against the potential-cycle number at electropolymerization. The surface coverage of the polymer increased proportionally with the cycle number up to about 80 cycles, with a polymer-growth rate of 5×10^{-11} mol cm^{-2} per cycle. As the potential cycle was repeated more than 100 times, however, Θ gradually approached a limiting value of 6×10^{-9} mol cm^{-2}. This result suggests a low rate of electron transport through the film, resulting from redox conduction.

Responding to the solution pH, the polymer was protonated and deprotonated. When the pH increased from one to seven, the $E_{1/2}$ of the polymer shifted to more negative potentials at a rate of 50 mV per unit pH (Fig.2). This change was similar to that (–57 mV/pH) observed for the monomeric dye incorporated into Nafion®, a perfluorosulfonated cation-exchange polymer. The latter rate is equal to that expected for the two-electron, two-proton reduction of MD^+ to the protonated leucoMeldola's blue MDH_2^+ (Scheme 1).

$$MD^+ + 2e + 2H^+ \rightarrow MDH_2^+ \qquad (2)$$

This observation implies that the polymer includes the same electroactive site as the monomer.

According to the published acid dissociation constant K_a for amino-substituted azines[38, 39], their oxidized forms are unprotonated at pH values above three: their basicity is weaker than that of aniline. In the present study, the pK_a of the conjugate acid of MD^+ was estimated to be less than 1 from the pH dependence of the absorbance at an absorption peak wavelength of 569 nm, where MD^+ showed a molar absorption coefficient of 1.7×10^4 $M^{-1}cm^{-1}$.

$$MDH^{2+} \rightarrow MD^+ + H^+ \qquad pK_a < 1 \qquad (3)$$

The molar absorption coefficient decreased when MD^+ was protonated in acid solutions. On the other hand, reduction of the azine rings generally makes their amino substituents more basic, thus inducing protonation of the amino groups[31, 38, 40, 41]. For example, protonated leucomethylene blue with a chemical structure similar to MDH_2^+ has been reported to have a pK_a of 5.6[23]. From these observations, one can safely state that the reduced Meldola's blue is protonated at weakly acidic pH values.

Previous studies[27] on the chemical structures of electropolymerized azines suggest that the amino nitrogen atom of one azine molecule link to a heterocyclic carbon atom of another such molecule (so-called head-to-tail bonding). Although our ATR-IR spectroscopic experiment failed to distinguish between the dimethylamino and ring-bridging amino groups, for two reasons we assume that PMD

includes the primary structure of phenoxazine (possibly with the tertiary amino group being demethylated[27]). First, the polymer had voltammetric properties like those of the dye (in $E_{1/2}$ and its pH dependence). Second, visible absorption band of the polymer disappeared upon its reduction, indicating the conversion of phenoxazine rings to unconjugated 10-hydro-phenoxazine rings. When the polymer is doubly reduced, thus, two protons will enter the polymer film in the pH range from 1 to 7. Being localized within the phenoxazine ring, its π-electrons are incapable of moving through the amino group that bridges the two rings. The electroactive properties of PMD can result from electron self-exchange between the isolated redox-active sites and from a high ionic conductivity of the polycationic material[37]. A slow rate of the electron hopping causes unsuccessful electrodeposition of PMD films thicker than 10^{-8} mol cm^{-2}. The high ionic conductivity is ascribed to a high concentration of charge-compensating counterions in the film. If the polymer film of $\Theta = 5.5 \times 10^{-9}$ mol cm^{-2} has a thickness of 17 nm, we can estimate the electroactive-site concentration at 3.2 M, neglecting the film swelling caused by water.

At the cycle number not exceeding 100, the electroactive polymer film indicated a log(I_{pc}) versus log(v) plot with a slope of 0.90 ± 0.08 (thin-film behavior) in the 2 to 200 mV s^{-1} range (the inset in Fig.2). In this study, hence, the PMD-modified electrode will be treated as a diffusionless system, that is, analyzed by the voltammetric theory for surface-confined species[42]. At sufficiently fast scan rates for the peak-to-peak separation $\Delta E_p > 0.2/n$ V to hold, the cathodic peak potential E_{pc} is given by

$$E_{pc} = E^{\circ\prime} - (RT/\alpha nF)\ln(\alpha nFv/RTk_s) \qquad (4)$$

where $E^{\circ\prime}$ is the formal potential, α is the transfer coefficient, k_s is the rate constant of a surface reaction (in s^{-1}), v is the scan rate, n is the number of electrons transferred in the heterogeneous reaction, and all other symbols have their usual meanings. If the condition for irreversible surface redox reactions is experimentally satisfied, Eq.(4) enables one to determine k_s from a variation in E_{pc} with v. Fig. 3 shows the potential difference ($E_{pc} - E^{\circ\prime}$) plotted against the logarithm of v for a 1.3 nmol cm^{-2} film in 0.2 M Na_2SO_4 solutions. The pH 0.7 solution yielded a linear ($E_{pc} - E^{\circ\prime}$) versus log(v) plot at higher scan rates than the pH 7 one did. The values of k_s and α were determined from the slope of the straight line and from its intercept with the horizontal line of ($E_{pc} - E^{\circ\prime}$) = 0. Table 1 lists the results obtained in an acidic and neutral solutions. When the solution pH increased from 0.7 to 7, k_s decreased to about one twenty, with α remaining near 0.5.

As can be seen from Eq.(2), the redox reaction of PMD has the pseudo-first-order rate constant including the proton concentration. Quick responses of I_{pc} and ΔE_p to the solution pH, examined in the pH range from 1 to 7, suggest rapid penetration of protons through the film. They move within polyazine

films through a Grotthus-type process, via water and/or amine sites in the polymers[43]. The potential-independent concentration of the supporting electrolyte can thus be distributed uniformly throughout the PMD film. Consequently, acidic solutions result in a high proton concentration in the film, increasing k_s. On the other hand, protonation of the polymer (causing a rise in its positive charge) raises the degree of swelling of the polymer film. This variation may increase the distance between redox-active sites, thus reducing k_s; however, this expectation is contrary to the experimental result. A high k_s value obtained in acidic solutions results from an increased proton concentration in the film.

3.2. Voltammetric characteristics of DA oxidation

Electrochemical properties of DA vary with the solution pH, because its oxidation corresponds to the change of 1,2-benzenediol into 1,2-benzoquinone. Fig. 4 illustrates typical cyclic voltammograms measured at a bare GC electrode in 1 mM DA solutions. At pH < 6, the electroactive species showed an oxidation and rereduction waves having a ΔE_p of 0.3 to 0.4 V at v = 200 mV s^{-1}, smaller than that observed at platinum electrodes. Because the conjugate acid of DA has a pK_a of 8.92[4], the pair of redox waves is assigned to the two-electron, two-proton conversion of protonated DA into the quinone form DAQ (Eq.(5), Scheme 2). When the pH was raised to 8, DA showed two additional waves: an anodic peak at 0.6 V and a cathodic at -0.3 V. The positive potential scan to 0.7 V greatly lowered the DA-regenerating peak appearing upon the reversed negative scan, indicating that the second electrooxidation is followed by a chemical reaction. According to previous studies[4, 11, 44], unprotonated DAQ is cyclized at the amine side chain into 5,6-dihydroxyindoline (Eq.(6), Scheme 2), which is further oxidized to indoline-5,6-quinone as shown by Eq.(7) (Scheme 2)[4, 11]. In the present study, the repetitive potential cycle between -0.3 and 0.7 V depressed voltammetric activity of the electrode gradually, because of the deposition of insoluble products. An electrode-poisoning effect of DA oxidation in neutral solutions has suggested that indoline-5, 6-quinone polymerizes to melanin-like compounds on electrode surfaces and thus impedes interfacial charge transfer[45]. The intramolecular cyclization made the following electrocatalytic oxidation of DA limit to pH values not more than 7.

It should be noted that the anodic peak potential E_{pa} of DA moved to more positive values with increasing its concentration (c_b). Fig. 5 shows E_{pa} versus c_b plots measured at a bare and PMD-modified electrodes in 0.2 M Na_2SO_4 solutions (pH 5). When c_b rose from 0.1 to 2 mM, E_{pa} changed from 0.30 to 0.42 V at v = 200 mV s^{-1} for the bare GC electrode, whereas it shifted gradually to less positive potentials for the chemically modified one. At the bare GC electrode, a similar change was observed for linear sweep voltammograms measured with a rotating disk electrode. The potential corresponding to a half of

the diffusion-limited current I_L moved to more positive values with an increase in c_b. In addition, this potential shifted similarly when the rotation speed ω rose from 1.67 to 66.7 Hz (Fig.10 (a)). These changes in potential noticed at the bare GC electrode can arise from the following reactions: (1) interfacial charge transfer accompanied with chemical reactions, (2) the association of DA molecules at higher concentrations to form aggregates, or (3) the adsorption of DA/DAQ on the GC surface. Although examining the changes in $I_{pa}/v^{1/2}$, E_{pa}, and I_{pa}/I_{pc} with v, we failed to characterize the mechanism of electrode reaction (5) aptly.

Because the third possibility is discussed in Section 3.3, let us consider the second possibility from the limiting current measured at the rotating disk electrode. For the pseudo-first-order redox reaction, this current increases proportionally with the square root of ω (units: Hz)[46]:

$$I_L = 1.554nFSD^{2/3}\eta^{-1/6}c_b\omega^{1/2} \quad (8)$$

where n denotes the total number of electrons transferred in the redox reaction of DA, D the diffusion coefficient of the species in an aqueous solution, and η its kinematic viscosity. A proportional relationship between I_L and $\omega^{1/2}$ allows one to evaluate D from the slope. As given in Fig. 6, all log I_L versus log ω plots measured in the concentration range from 0.1 to 4 mM show linear lines with a slope of 0.49 ± 0.06. When plotted against c_b, the slopes of I_L versus $\omega^{1/2}$ plots increase proportionally with the concentration (the inset in Fig. 6); thus, oxidation of DA obeys good first-order kinetics. Equation (8) gives a constant D of 6.5×10^{-6} cm^2s^{-1}, which agrees with the value reported by Chen and Cha[7]. These results indicate that DA does not form any aggregates in the concentration range examined.

3.3. Electrocatalytic oxidation of DA at PMD-modified electrodes

3.3.1. Influence of PMD films on the kinetic parameters of DA oxidation

The redox polymer heightened the anodic peak current I_{pa} of DA measured by cyclic voltammetry. Fig. 7 shows typical cyclic voltammograms observed at a polyazine-modified and bare electrodes in a 1 mM DA solution containing 0.2 M Na_2SO_4. Poly(methylene blue) hardly enhanced the current of DA oxidation at any pH values, shifting the current peak to more positive potentials (Fig.7 a). On the other hand, PMD raised I_{pa} of DA by a factor of 5 to 6 at a c_b of 1 mM (Fig.7 b). However, its effect depended on the DA concentration. At the PMD-modified electrode, I_{pa} of DA increased rapidly as c_b rose from 0 to 0.2 mM, above which it approached a limiting value. At the bare GC electrode, I_{pa} of DA increased linearly with c_b up to 5 mM, indicating the first-order dependence on the concentration. As a result, the

ratio of the catalyzed to uncatalyzed peak currents dropped from 10 to 1 as c_b rose from 0.1 to 5 mM (the inset in Fig. 7 b).

The polymer-enhanced current will allow one to detect DA at concentrations of the order of 5 μM by differential pulse voltammetry, which excludes capacitive currents effectively and gives peak-shaped polarization curves. Fig. 8 shows both the differential pulse voltammograms and calibration plot for the electrocatalytic oxidation occurring in dilute DA solutions. On renewed polymer film surfaces, I_{pa} had an standard error of about ± 60% at 2 μM DA and not less than ± 100% at 1 μM. Hence, the PMD-modified electrode enables one to determine DA quantitatively in the concentration range of 5 to 20 μM by the pulse technique, with a detection limit of 3 μM.

Rotating disk electrode voltammetry gives the well-defined solution hydrodynamics and thus involves the simplest theoretical derivations for the kinetic analysis of electrocatalytic reactions. In this stationary technique, we evaluated the rate constant of DA oxidation by using a PMD film with a Θ of (4.8 - 6.1) × 10^{-9} mol cm^{-2} (showing thin-film behavior) to ensure fast charge transport through the polymer. For mixed kinetic-diffusion control where the current I depends on the electrode potential E, I is given by [47)]

$$I = (1 - I/I_L)I_k \tag{9}$$

where I_k is the kinetic current corresponding to the rate of interfacial charge transfer. Because the DA concentration at the electrode surface is zero at much more positive potentials than $E°'$, I is determined by mass transport to the surface. From Eqs.(8) and (9), one obtains

$$1/I = 1/I_k + (1.554nFSD^{2/3}\eta^{-1/6}c_b\omega^{1/2})^{-1} \tag{10}$$

The plot of I^{-1} against $\omega^{-1/2}$ thus enables one to evaluate I_k from the intercept at $\omega = \infty$. At anodic potentials where the reverse process is ignored, I_k can be written as

$$I_k = nFSk°c_b \exp[\alpha n_a F(E - E°')/RT] \tag{11}$$

where $k°$ is the apparent standard heterogeneous rate constant including the proton concentration and n_a is the number of electrons involved in the rate-determining step. If the logarithm of I_k increases linearly with $(E - E°')$, then one can estimate $k°$ and αn_a.

The rotating-disk voltammetric results obtained at the bare GC electrode indicated that Eq.(5)

comprised plural steps where one electron was transferred in the rate-determining step. Fig. 9 (a) shows the I^{1} versus $\omega^{-1/2}$ plots for the bare GC electrode in a 0.2 mM DA solution (pH 6). At less positive potentials, a linear relationship was observed only in the higher ω range, as predicted from the voltammograms in Fig. 10 (a). The plots measured at more positive potentials, on the other hand, indicated a well-behaved linear relationship. The logarithm of I_k determined from the intercept at $\omega = \infty$ is plotted against E in the inset in Fig. 9 (a). At much more positive potentials than $E°'$, the plots deviated from a straight line because I approached I_L. For the 0.2 - 2 mM DA solutions buffered at pH 6, we estimated $k°$ at $(3.9 \pm 0.7) \times 10^{-4}$ cm s^{-1} and αn_a at 0.38 ± 0.08 from Eq.(11). The latter value suggests that one electron be transferred in the rate-determining step. If assuming $n_a = 2$, then we obtain an α of 0.19 which is uncommon value[48]. A similar αn_a value of 0.40 was cyclic-voltammetrically obtained from a linear change in E_{pa} with the logarithm of v in the range from 0.2 to 10 V s^{-1}. The result just mentioned is consistent with the suggestion that electrochemical oxidation of DA to DAQ proceeds via two consecutive one-electron transfer processes with the intermediate semiquinone[4].

Voltammetric sensing based on polymer-modified electrodes depends largely on how rapidly the polymer films communicate the electric signals stemming from target recognition to the underlying electrodes. Fig. 10 (b) shows the linear sweep voltammograms of DA measured at a rotating PMD-modified electrode in a 0.2 mM DA solution (pH 6). The polymer film shifted the $E_{1/2}$ of DA to less positive values (compare with the voltammograms in Fig.5), with I_L remaining unchanged. Moreover, the current rose to the limiting value in a narrow potential range compared with that for the bare GC electrode. Fig. 9 (b) presents I^{-1} versus $\omega^{-1/2}$ plots measured at various potentials. The polymer-coated electrode established a linear relationship between I^{-1} and $\omega^{-1/2}$ in the wider ω range than the bare one did. The logarithm of I_k determined by extrapolation of the straight line is plotted as a function of E in the inset in Fig. 9 (b). For a 0.2 mM DA solution (pH 6), we estimated $k°$ at 5.0×10^{-3} cm s^{-1} and αn_a at 0.98 (which yields $\alpha = 0.49$ for $n_a = 2$) from the straight line shown in the inset. This $k°$ value is an order of magnitude higher than that measured at the bare GC electrode. In addition, the polymer film increased the dependence of I_k on E probably by enabling a two-electron transfer step. The apparent standard heterogeneous rate constant is plotted against c_b in Fig. 11. It decreased as c_b was raised to more than 0.5 mM, corresponding with the limiting I_{pa} observed at high concentrations.

Because both the redox reactions of DA and PMD include protons, the polymer film can change the dependence of $k°$ on the solution pH. In practice, further oxidation of DA to occur in basic solutions made the reliable determination of $k°$ limit to aqueous media more acidic than pH 7. Table 2 summarizes the results of the rotating disk electrode voltammetry performed at three different pH values. Whereas the rate constant obtained at the bare GC electrode remains almost unchanged, that measured

at the polymer-modified electrode tends to decrease as the solution is acidified.

3.3.2. Interpretation of the electrocatalytic effect

Because the $E\,°'$ of the DA/DAQ couple (0.16 V at pH 7) is more positive than that of the MD^+/MDH couple (-0.19 V at pH 7), electron cross-exchange (12) is thermodynamically unfavorable,

$$MD^+ + DA \rightarrow MDH + DAQ \tag{12}$$

that is, its standard Gibbs energy change $\Delta G° = 2F\,[E°'(\mathrm{DA/DAQ}) - E°'(MD^+/\mathrm{MDH})] > 0$. Hence, the electrocatalytic oxidation of DA at PMD-modified electrodes should be attributed to other causes than the cross-exchange reaction.

It should be noted that the polyelectrolyte film extracted DA from aqueous electrolyte solutions. When having been soaked in 0.5 mM DA solutions for 1 hr, the polymer-modified electrode indicated the anodic wave (at about 0.4 V at pH 5) due to the DA incorporated into the film. The surface concentration Γ of DA calculated from the area under the wave was on the order of 4×10^{-10} mol cm^{-2} for a PMD film having a surface coverage of 5.4×10^{-9} mol cm^{-2}. Assuming that the film is 17 nm thick, we can estimate the DA concentration in the film at 2.4×10^{-4} mol cm^{-3} from the Γ value. When the loaded film was soaked in a pure electrolyte solution, however, Γ decreased at a rate of 6–7% per minute. This decrease indicates that the DA incorporated was gradually released from the polymer during the slow potential scan. Thus, Γ values measured by this method were underestimated.

The surface concentration at equilibrium was determined by potential-step chronocoulometry, assuming that the film has as small thickness as submonolayers. Voltammetric charge Q versus time t curves measured at long times and a large-amplitude potential step are expressed by the Cottrell equation[43]:

$$Q = Q_a + 2nFSc_b(Dt/\pi)^{1/2} \tag{13}$$

where Q_a denotes the charge for oxidizing the electroactive species adsorbed on the electrode surface. Fig. 12 shows typical Q versus $t^{1/2}$ plots for a potential step from 0.25 to 0.65 V at pH 4. For bare electrodes (the inset), the charge corrected for the residual charge at $c_b = 0$ varied linearly with $t^{1/2}$ in the time range from 10 ms to 1 s, as expected for a diffusion-limited process. The straight line extrapolated to zero time allows us to estimate both D from the slope and Γ from the intercept $Q_a = nFS\Gamma$. The diffusion coefficient estimated from the slope corresponded to a value of $(5.8 \pm 1.3) \times 10^{-6}$ cm^{2}s^{-1},

agreeing closely with that determined by the rotating disk voltammetry. Fig. 13 shows Γ plotted as a function of c_b. The chronocoulometric result indicated that DA is adsorbed onto the GC surface up to about 4×10^{-11} mol cm^{-2}. This interaction can be related to the ΔE_p values smaller than those measured at platinum electrodes. The polymer-modified electrodes, on the other hand, showed linear Q versus $t^{1/2}$ plots except for the early stages of the measurement (< 20 ms), with the intercept differing greatly from zero. The deviation for a longer period than that observed at the bare electrode can result from mass transport in the film. The surface concentration calculated from the intercept is plotted against c_b in Fig. 13. It increases consistently up to 0.5 mM and then approaches to a limiting value. Hence, it is reasonable to conclude that the decrease in $k°$ with c_b results from a limited DA concentration in the film. The distribution constant of DA between the film and solution was roughly estimated at 3000 from the slope of the linear segment at low concentrations in Fig. 13. The limiting surface concentration measured for the modified electrode is an order of magnitude higher than that obtained for the bare electrode. Consequently, the increases in $k°$ and αn_a due to the surface modification can be ascribed to the binding interaction of DA with the polymer film. It is noteworthy that this interaction accelerates the two-electron transfer step.

To clarify a binding interaction between DA and the polymer, we discuss whether Γ is affected by the ionic charge of the polymer or not. The surface concentration in the polymer film equilibrated with a 0.5 mM DA solution is plotted against its pH in the inset in Fig.13. It decreased as the pH was varied from 5 to 0.7. When protonated in strongly acidic solutions, the polymer weakened the binding interaction with the protonated DA probably because of electrostatic repulsion between the two positively charged species. Thus, the chemical interaction of DA with PMD plays a key role in the incorporation of the neurotransmitter with the polyelectrolyte film.

4. Conclusions

The present study leads to the following conclusions.

1. Whereas poly(methylene blue) hardly enhances the current of DA oxidation, PMD raises I_{pa} by a factor of 10 at low c_b values. This electrocatalytic effect of PMD enables one to detect DA at concentrations of the order of 5 μM.

2. Because the rate of electron hopping in PMD is slower than that in poly(methylene blue), the electrocatalytic activity is independent of electron self-exchange between neighboring redox-active sites.

3. The PMD film on electrode surfaces increases the $k°$ of DA oxidation more than 10-fold and promotes the two-electron transfer step, thus raising the dependence of I_k on the potential.

4. The increases in k° and αn_a due to the electrode modification arise from the incorporation of DA with the polymer. Its protonation decreases the adsorption of DA to the film. A full understanding of the mechanism of the incorporation requires spectroscopic studies of a chemical interaction between DA and the polyelectrolyte.

References

1) J. Wang and A. Walcarius, *J. Electroanal. Chem.*, **407**, 183 (1996).

2) D.M. Zhou, H.X. Ju and H.Y. Chen, *J. Electroanal. Chem.*, **408,** 219 (1996).

3) T.F. Kang, G.L. Shen and R.Q. Yu, *Talanta*, **43,** 2007 (1996).

4) X.L. Wen, Y.H. Jia and Z.L. Liu, *Talanta*, **50,** 1027 (1999).

5) K. Takehara, H. Takemura, M. Aihara and M. Yoshimura, *J. Electroanal. Chem.*, **404,** 179 (1 996).

6) S. Cosnier, C. Innocent, L. Allien, S. Poitry and M. Tsacopoulos, *Anal. Chem.*, **69**, 968 (1997).

7) J. Chen and C.S. Cha, *J. Electroanal. Chem.*, **463**, 93 (1999).

8) A. Cizewski and G. Milczarek, *Anal. Chem.*, **71,** 1055 (1999).

9) Z. Xun, C. Cai, W. Xing and T. Lu, *J. Electroanal. Chem.*, **545,** 19 (2003).

10) H. Razmi, M. Agazadeh and B. Habibi-A, *J. Electroanal. Chem.*, **547,** 25 (2003).

11) S.M. Chen and K.T. Peng, *J. Electroanal. Chem.*, **547,** 179 (2003).

12) T.F. Kang, G.L. Shen and R.Q. Yu, *Anal. Chim. Acta*, **354,** 343 (1997).

13) J. Oni and T. Nyokong, *Anal. Chim. Acta*, **434**, 9 (2001).

14) M.D. Rubianes and G.A. Rivas, *Anal. Chim. Acta*, **440,** 99 (2001).

15) A. Dalmia, C.C. Liu and R.F. Savinell, *J. Electroanal. Chem.*, **430,** 205 (1997).

16) H. Zhao, Y. Zhang and Z. Yusan, *Analyst* **126**, 358 (2001).

17) F. Xu, M. Gao, L. Wang, G. Shi, W. Zhang, L. Jin and J. Jin, *Talanta*, **55**, 329 (2001).

18) L. Zhang, Y. Sun and X. Lin, *Analyst*, **126**, 1760 (2001).

19) H. Zhao, Y. Zhang and Z. Yusan, *Anal. Chim. Acta*, **441,** 117 (2002).

20) Q. Wang, D. Dong and N. Li, *Bioelectrochemistry*, **54**, 169 (2001).

21) L.L. Miller and Q.X. Zhou, *Macromolecules*, **20**, 1594 (1987).

22) B. Piro, T.A. Nguyen, J. Tanguy and M.C. Pham, *J. Electroanal. Chem.*, **499,** 103 (2001).

23) S.L.P. Dias, S.T. Fujiwara, Y. Gushikem and R.E. Bruns, *J. Electroanal. Chem.*, **531**, 141 (2002).

24) P. Sevcík and H.B. Dunford, *J. Phys. Chem.*, **95,** 2411 (1991).

25) S.A. Wring and J.P. Hart, *Analyst*, **117**, 1215 (1992).

26) F. Ni, H. Feng, L. Gorton and T.M. Cotton, *Langmuir*, **6,** 66 (1990).

27) A.A. Karyakin, E.E. Karyakina and H.-L. Schmidt, *Electroanalysis*, **11**, 149 (1999).

28) A.A. Karyakin, E.E. Karyakina, W. Schuhmann and H.-L. Schmidt, *Electroanalysis*, **11**, 553 (1999).

29) C.X, Cai and K.H. Xue, *J. Electroanal. Chem.*, **427,** 147 (1997).

30) R. Yang, C. Ruan, W. Dai, J. Deng and J. Kong, *Electrochim. Acta*, **44,** 1585 (1999).

31) G. Inzelt and E. Csahók, *Electroanalysis*, **11,** 744 (1999).

32) D. Benito, C. Gabrielli, J.J. Garcia-Jareno, M. Keddam, H. Perrot and F. Vincente, *Electrochem. Commun*., **4,** 613 (2002).

33) C.M.A. Brett, G. Inzelt and V. Kertész, *Anal. Chim. Acta*, **385**, 119 (1999).

34) Y. Ye and R. Baldwin, *Anal. Chem.*, **60,** 2263 (1988).

35) M.J. Lobo, A.J. Miranda and P. Tuñon, *Electroanalysis*, **9**, 191 (1997).

36) M. Ohtani, S. Kuwabata and H. Yoneyama, *J. Electroanal. Chem.*, **422,** 45 (1997).

37) T. Komura, G.Y. Niu and T. Yamaguchi, *Electroanalysis*, in press.

38) K. Hutchinson, R.E. Hester, W.J. Albery and A.R. Hillman, *J. Chem. Soc. Faraday Trans. 1*, **80,** 2053 (1984).

39) Z. Ping, G.E. Nauer, H. Neugebauer and J. Theiner, *J. Electroanal. Chem.* **420**, 301(1997).

40) D.M. Zhou, J.J. Sun, H.Y. Chen and H.Q. Fang, *Electrochim. Acta*, **408,** 1803 (1998).

41) S. Bruckenstein, C.P. Wilde and A.R. Hillman, *J. Phys. Chem.*, **94**, 6458 (1990).

42) E. Laviron, *J. Electroanal. Chem.*, **101**, 19 (1979).

43) M.E.G. Lyons, *Electroactive Polymer Electrochemistry, Part 1* (Ed. M.E.G. Lyons), Plenum Press, New York, p.1, (1994).

44) M.D. Hawley, S.V. Tatawawadi, S. Piekarski and R.N. Adams, *J. Am. Chem. Soc.*, **89,** 447 (1967).

45) R.F. Lane and A.T. Hubbard, *Anal. Chem.*, **48,** 1287 (1976).

46) L. Gorton, A. Torstensson, H. Jaegfeldt and G. Johansson, *J. Electroanal. Chem*., **161**, 103 (1984).

47) Ref. 43, p.237.

48) A.J. Bard and L.R. Faulkner, *Electrochemical Methods*, Wiley, New York, p.95, (1980).

Figure Captions

Table 1 Rate constants of the surface redox reaction of PMD

Table 2 Rate constants of the oxidation of 0.2 mM DA at different pH values

Structure 1 Azines used in the present work.

Scheme 1 Redox reaction of Meldola's blue.

Scheme 2 Possible scheme for oxidation of DA.

Fig. 1 Cyclic voltammogram measured at a PMD-modified electrode in a 0.2 M H_2SO_4 solution. Θ = 5.1×10^{-9} mol cm^{-2} (the potential-cycle number at electropolymerization = 100), v = 10 mV/s. The inset shows an increase in I_{pc} with the potential-cycle number at electropolymerization. v = 5 mV/s.

Fig. 2 Half-wave potential plotted against the solution pH (the straight line shown has a slope of -50 mV/pH). The inset shows a log-log plot of I_{pc} versus v, with a slope of 0.91. $\Theta = 5.7 \times 10^{-9}$ mol cm^{-2}, a 0.2 M H_2SO_4 solution.

Fig. 3 Changes in E_{pc} with the logarithm of v for a pH 7 (○) and 0.7 (□) solutions. $\Theta = 1.3 \times 10^{-9}$ mol cm^{-2}.

Fig. 4 Typical cyclic voltammograms measured at a bare electrode in 1 mM DA solutions buffered at pH 5 (—) and 8 (-----). v = 100 mV/s.

Fig. 5 Changes in E_{pa} with c_b observed at a bare (○) and a PMD-modified (◊) electrodes in 0.2 M Na_2SO_4 solutions (pH 5). v = 200 mV/s.

Fig. 6 Log-log plots of I_L versus ω measured at a bare electrode in the pH 6 solutions of different DA concentrations. The inset shows a linear relationship between c_b and the slope of I_L-$\omega^{1/2}$ plots.

Fig. 7 Typical cyclic voltammograms observed at a polyazine-modified (solid line) and bare GC (broken line) electrodes in a 1 mM DA solution containing 0.2 M Na_2SO_4. v = 100 mV/s. (a)

poly(methylene blue) (PMT); (b) PMD. The inset in Fig. 7b shows a rapid decrease in the catalytic current with c_b.

Fig. 8 Differential pulse voltammograms at progressively higher concentrations of DA and calibration plot for the electrocatalytic oxidation in dilute DA solutions.

Fig. 9 Plots of I^{-1} against $\omega^{-1/2}$ measured at different potentials for (a) the bare GC electrode and (b) the PMD-modified one in a 0.2 mM DA solution (pH 6). Measured potentials: (a) (○) 0.37 V, (●) 0.40, (Δ) 0.45, (□) 0.50, and (◊) 0.60; (b) (○) 0.25 V, (●) 0.275, (Δ) 0.30, (□) 0.325, and (◊) 0.35. Insets of (a) and (b) show the logarithm of I_k plotted against E respectively.

Fig. 10 Linear sweep voltammograms of a 0.2 mM DA solution (pH 6) measured at (a) a bare GC electrode and (b) a PMD-modified one rotating at various rotation speeds/Hz.

Fig. 11 Standard heterogeneous rate constant plotted against c_b. pH 6.

Fig. 12 Typical potential step Q versus $t^{1/2}$ plots measured at the PMD-modified electrode in the pH 4 solutions of different DA concentrations. The inset shows Q versus $t^{1/2}$ plots measured at the bare GC electrode.

Fig. 13 Plots of Γ against c_b measured at pH = 4. (◊) bare GC electrode and (○) PMD-modified one. The inset shows the relationship between the solution pH and the Γ of DA adsorbed from 0.5 mM solutions.

Table 1. Rate constants of the surface redox reaction of PMD

	$E_{1/2}$ /V	v_c /mV s^{-1}	k_s /s^{-1}	α
pH 0.7	0.171	320	13.9	0.55
7	-0.141	17	0.62	0.48

Takahiro YAMAGUCHI*, Teruhisa KOMURA, Sayomi HAYASHI, Manabu ASANO, Guang Yao NIU, Kohshin TAKAHASHI

Table 2. Rate constants of the oxidation of 0.2 mM DA at different pH values

	bare GC		PMD-modified electrode	
	αn_a	$k°$/(cm s^{-1})	αn_a	$k°$/(cm s^{-1})
pH 6	0.38	3.9×10^{-4}	0.98	5.0×10^{-3}
pH 4	0.44	4.2×10^{-4}	0.94	4.5×10^{-3}
pH 2	0.46	4.6×10^{-4}	0.86	2.1×10^{-3}

Takahiro YAMAGUCHI*, Teruhisa KOMURA, Sayomi HAYASHI, Manabu ASANO, Guang Yao NIU, Kohshin TAKAHASHI

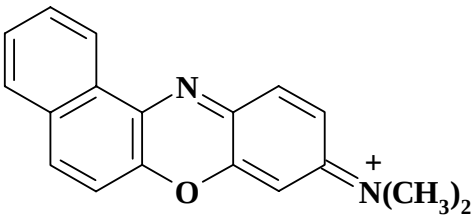

Meldola's blue

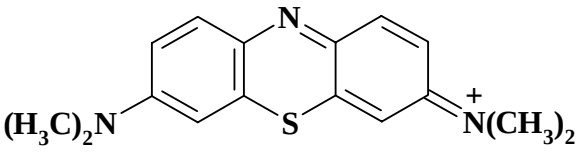

Methylene blue

Structure 1

Takahiro YAMAGUCHI*, Teruhisa KOMURA, Sayomi HAYASHI, Manabu ASANO, Guang Yao NIU, Kohshin TAKAHASHI

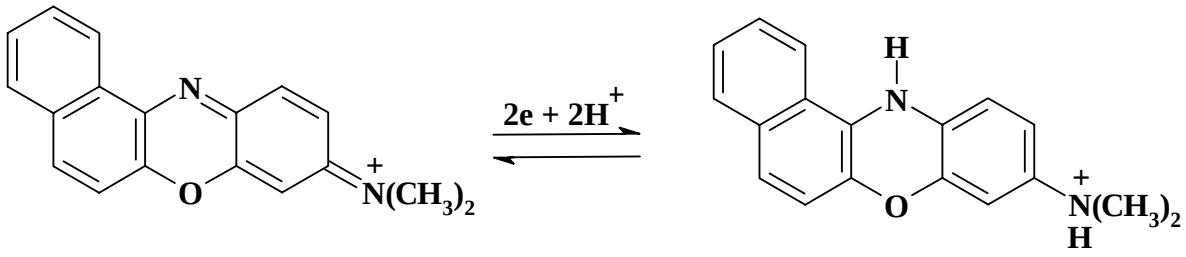

Scheme 1

Takahiro YAMAGUCHI*, Teruhisa KOMURA, Sayomi HAYASHI, Manabu ASANO, Guang Yao NIU, Kohshin TAKAHASHI

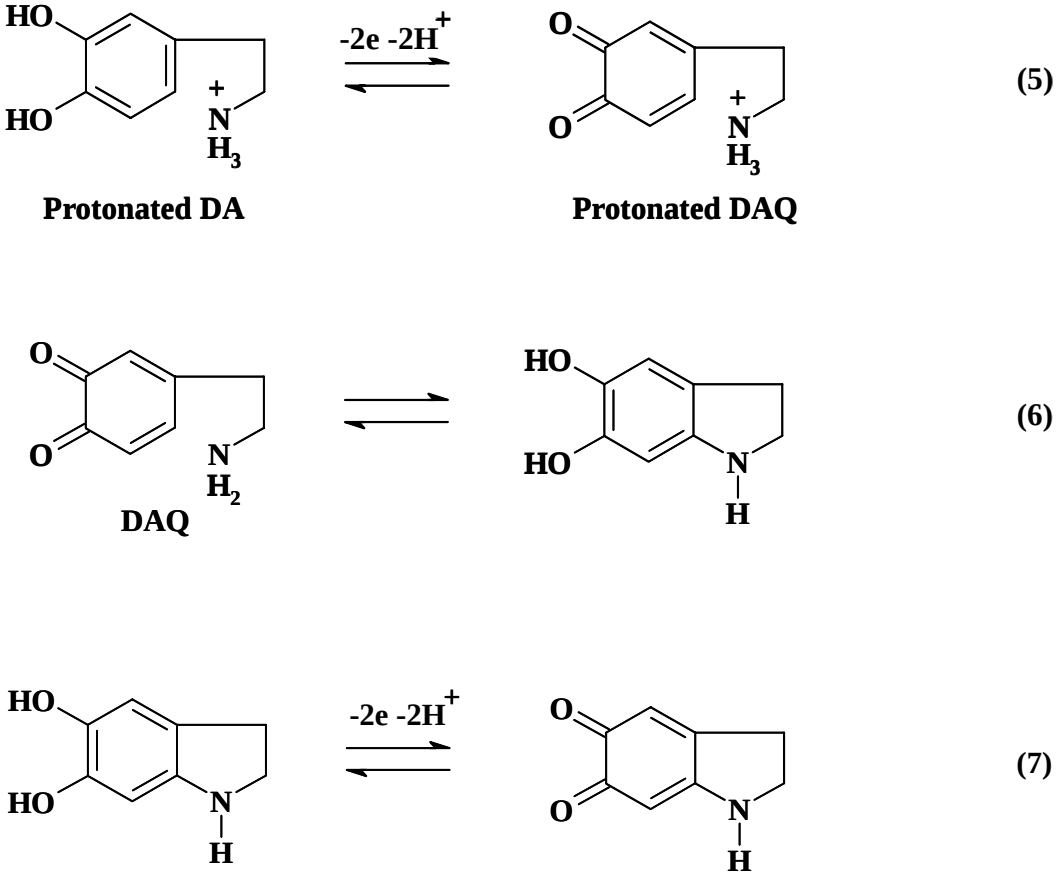

Scheme 2

Takahiro YAMAGUCHI*, Teruhisa KOMURA, Sayomi HAYASHI, Manabu ASANO, Guang Yao NIU, Kohshin TAKAHASHI

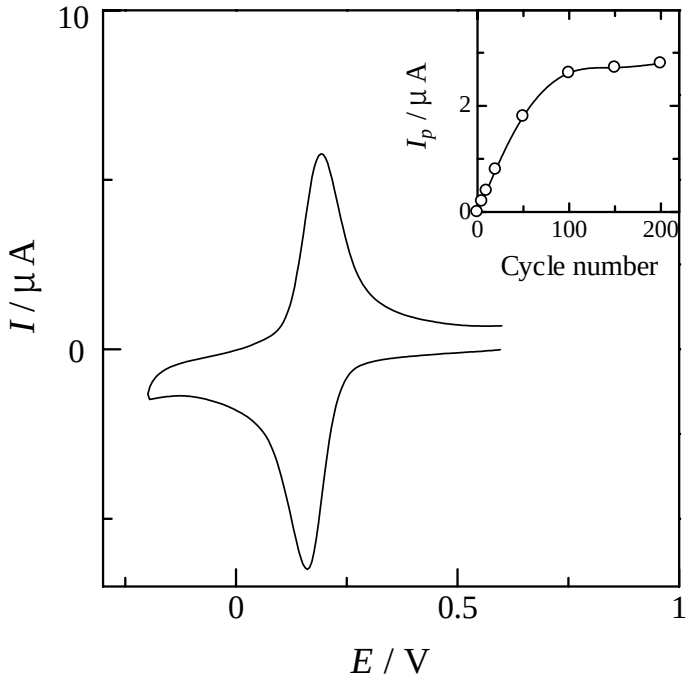

Fig. 1

Takahiro YAMAGUCHI*, Teruhisa KOMURA, Sayomi HAYASHI, Manabu ASANO, Guang Yao NIU, Kohshin TAKAHASHI

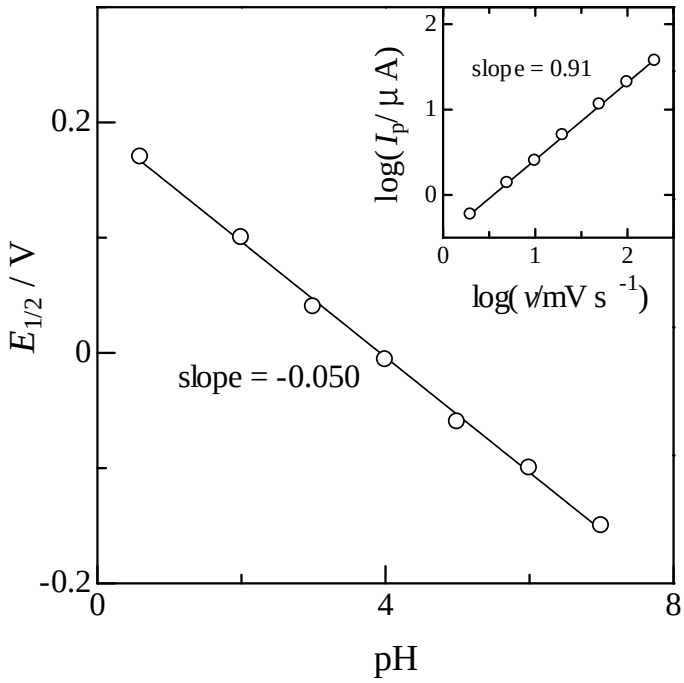

Fig. 2

Takahiro YAMAGUCHI*, Teruhisa KOMURA, Sayomi HAYASHI, Manabu ASANO, Guang Yao NIU, Kohshin TAKAHASHI

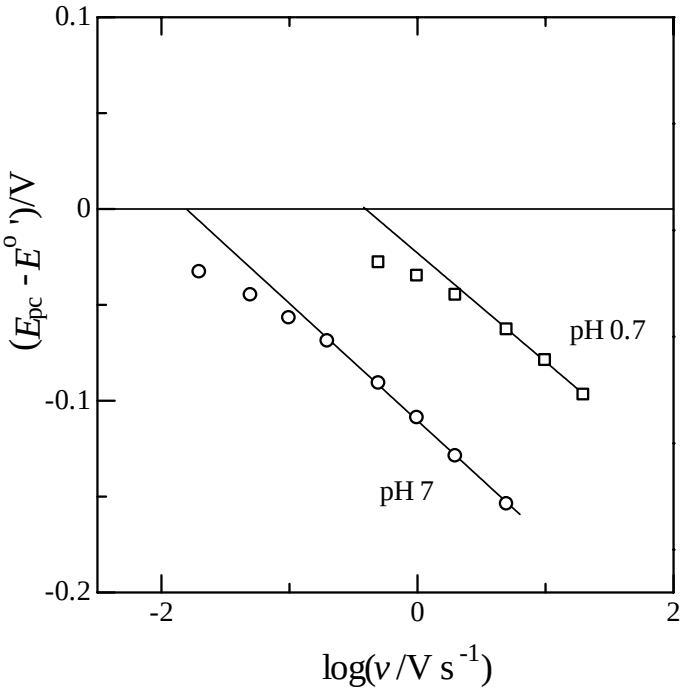

Fig. 3

Takahiro YAMAGUCHI*, Teruhisa KOMURA, Sayomi HAYASHI, Manabu ASANO, Guang Yao NIU, Kohshin TAKAHASHI

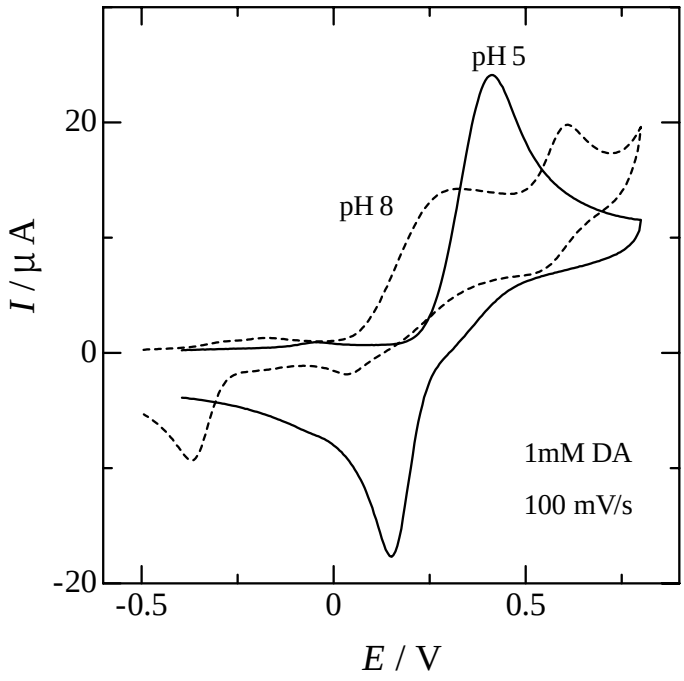

Fig. 4

Takahiro YAMAGUCHI*, Teruhisa KOMURA, Sayomi HAYASHI, Manabu ASANO, Guang Yao NIU, Kohshin TAKAHASHI

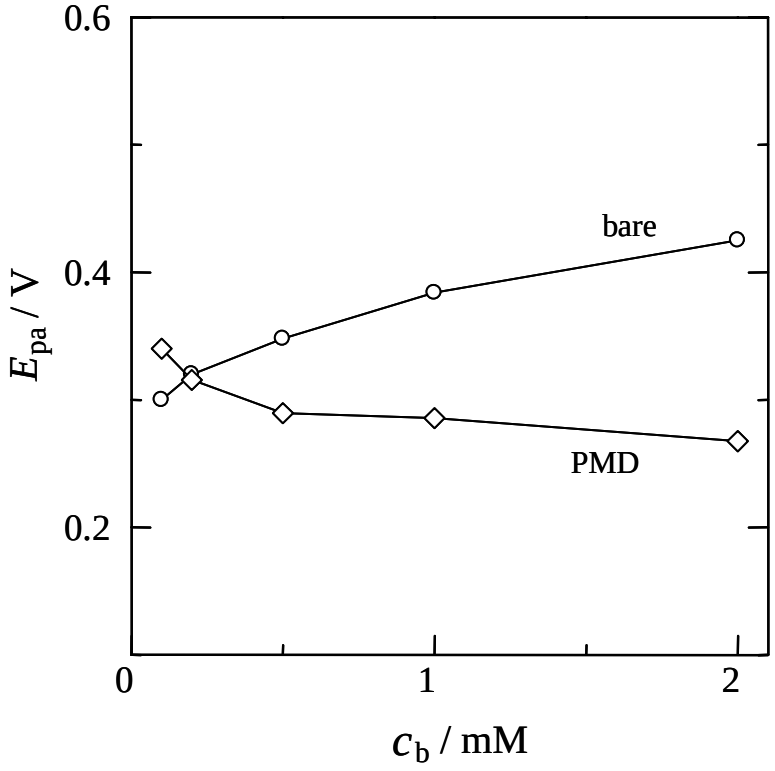

Fig. 5

Takahiro YAMAGUCHI*, Teruhisa KOMURA, Sayomi HAYASHI, Manabu ASANO, Guang Yao NIU, Kohshin TAKAHASHI

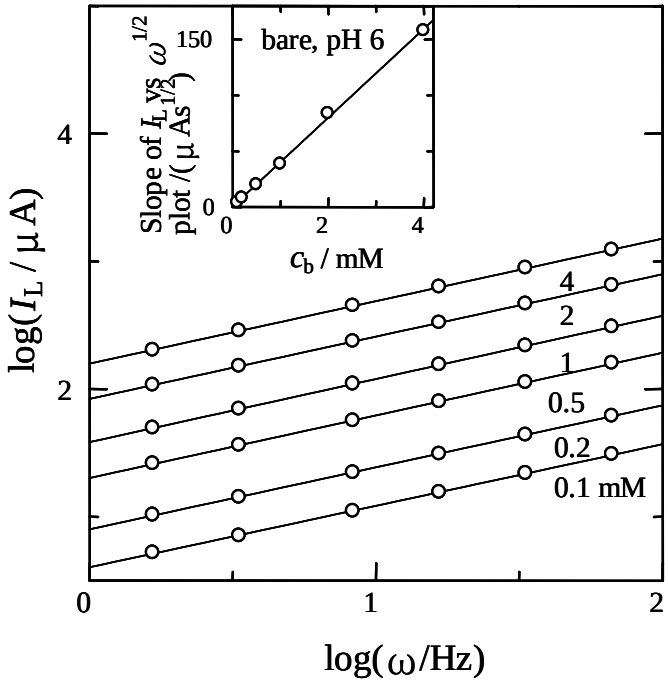

Fig. 6

Takahiro YAMAGUCHI*, Teruhisa KOMURA, Sayomi HAYASHI, Manabu ASANO, Guang Yao NIU, Kohshin TAKAHASHI

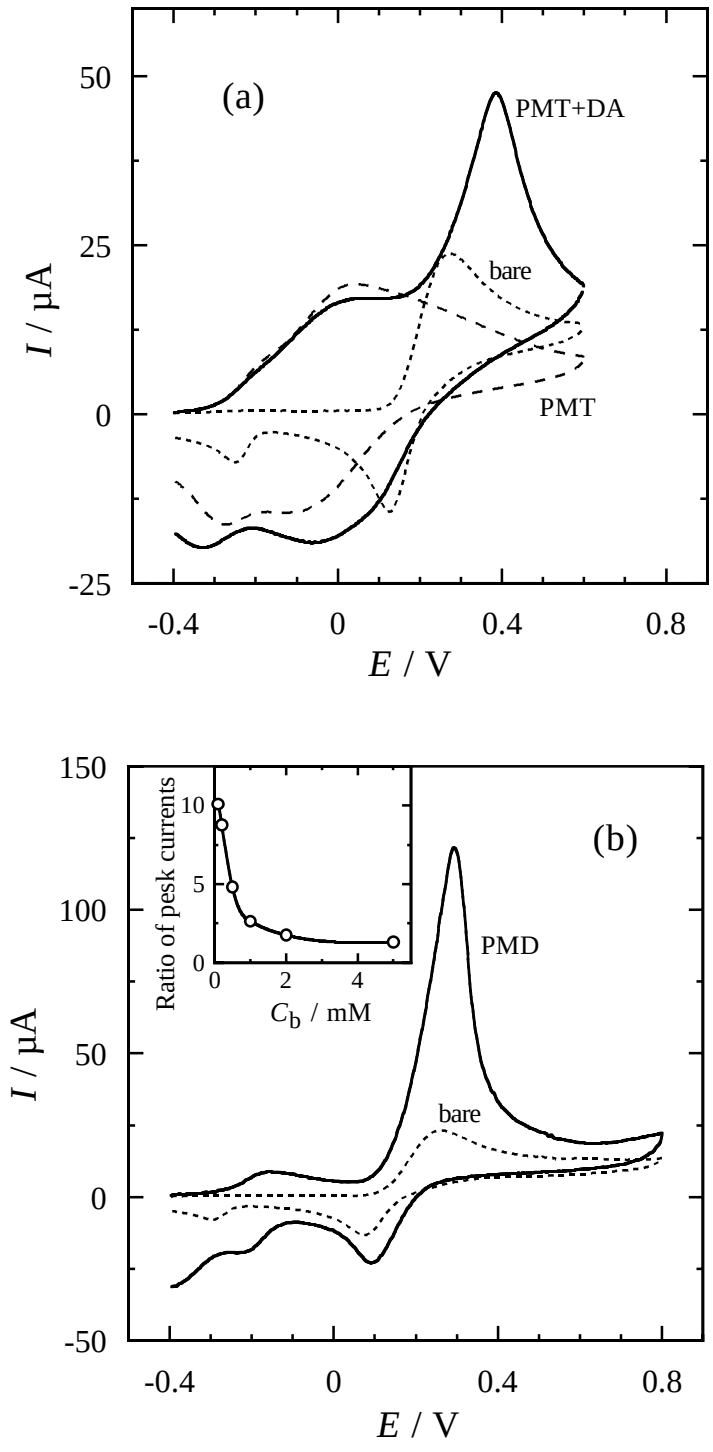
(a)
PMT+DA
bare
PMT
50
25
0
-25
-0.4
0
0.4
0.8
I / μA
E / V
(b)
PMD
bare
150
100
50
0
-50
Ratio of pesk currents
10
5
0
0
2
4
C_b / mM

Fig. 7

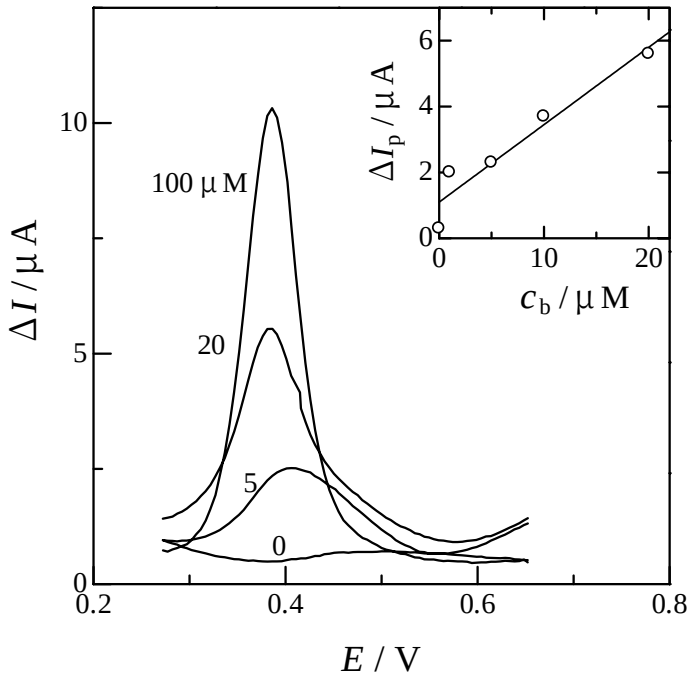

Fig. 8

Takahiro YAMAGUCHI*, Teruhisa KOMURA, Sayomi HAYASHI, Manabu ASANO, Guang Yao NIU, Kohshin TAKAHASHI

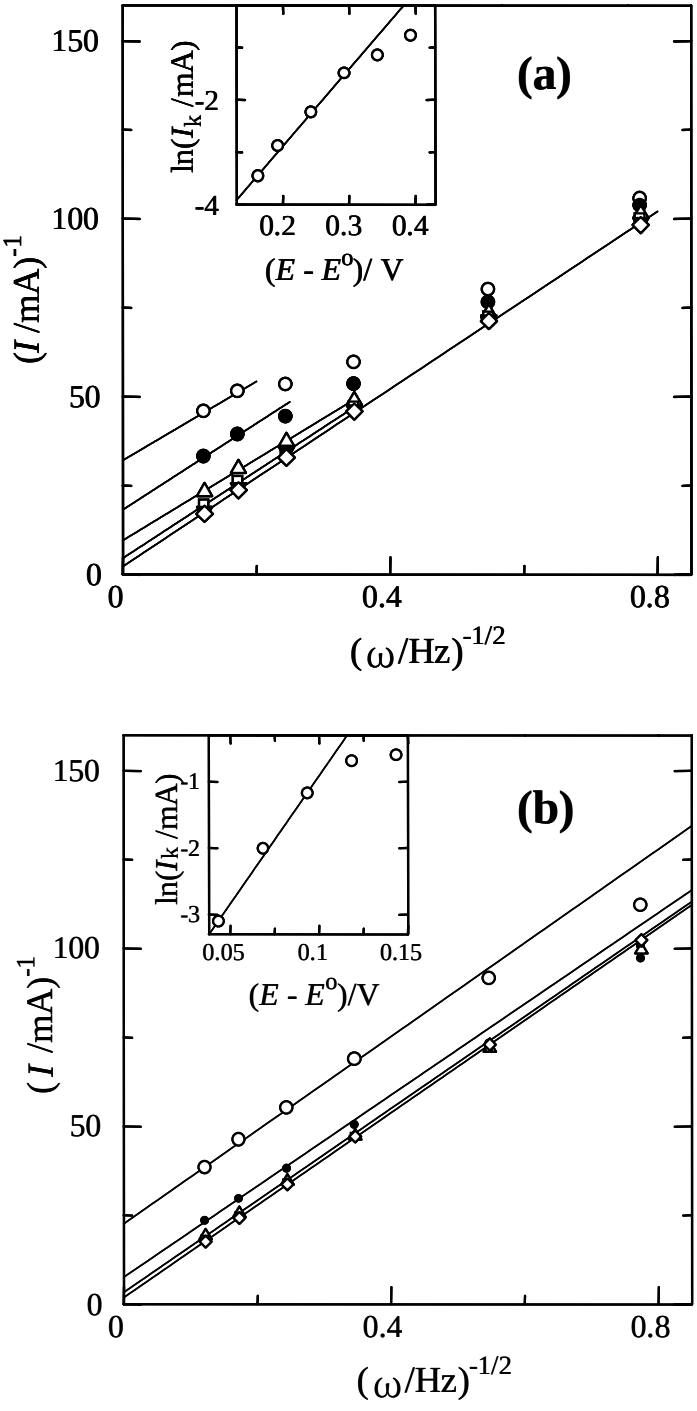
(a)
150
100
50
0
0
0.4
0.8
$(I/\mathrm{mA})^{-1}$
$(\omega/\mathrm{Hz})^{-1/2}$
$\ln(I_k/\mathrm{mA})$
-2
-4
0.2
0.3
0.4
$(E - E^o)/\ V$
(b)
150
100
50
0
0
0.4
0.8
$(I/\mathrm{mA})^{-1}$
$(\omega/\mathrm{Hz})^{-1/2}$
$\ln(I_k/\mathrm{mA})$
-1
-2
-3
0.05
0.1
0.15
$(E - E^o)/\mathrm{V}$

Fig. 9

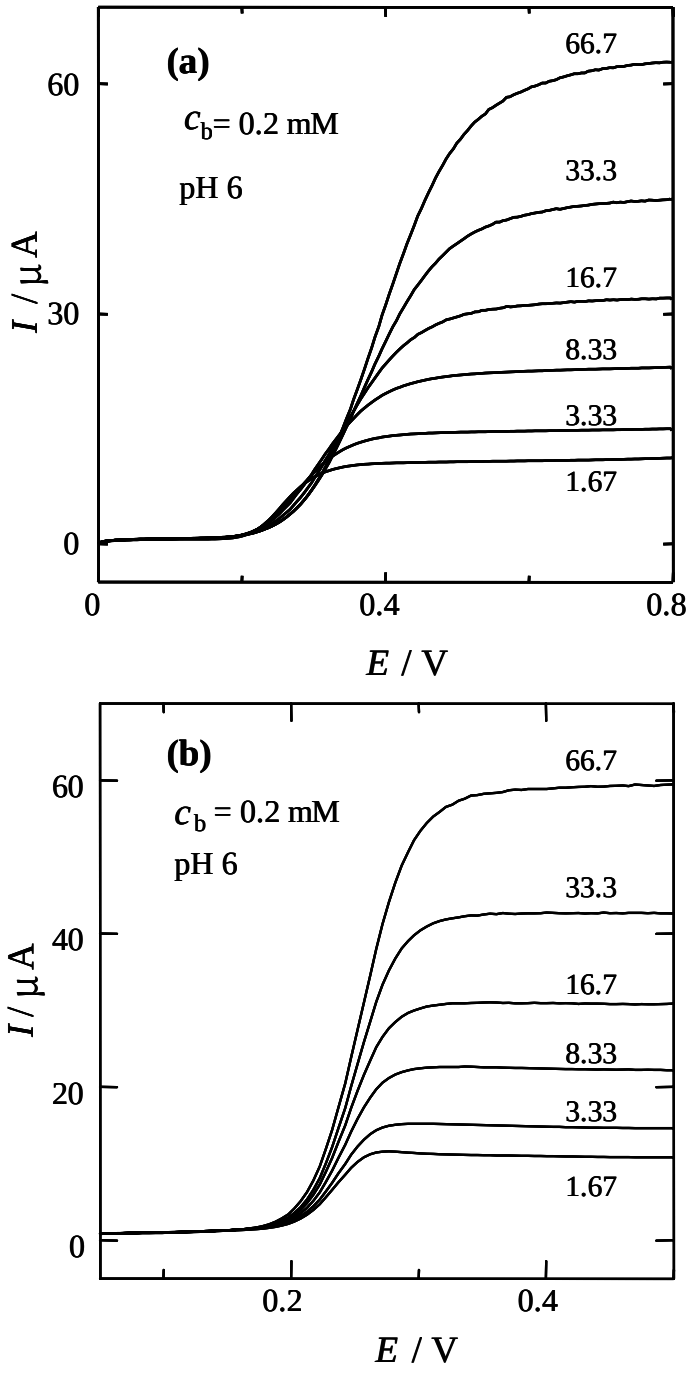
(a)
c_b= 0.2 mM
pH 6
66.7
33.3
16.7
8.33
3.33
1.67
60
30
0
0
0.4
0.8
I / μA
E / V
(b)
c_b = 0.2 mM
pH 6
66.7
33.3
16.7
8.33
3.33
1.67
60
40
20
0
0.2
0.4
I / μA
E / V

Fig. 10

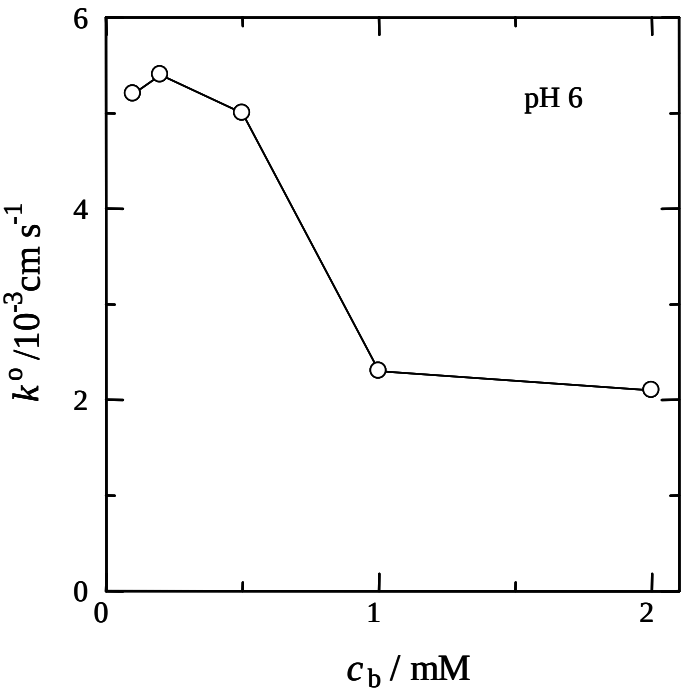

Fig. 11

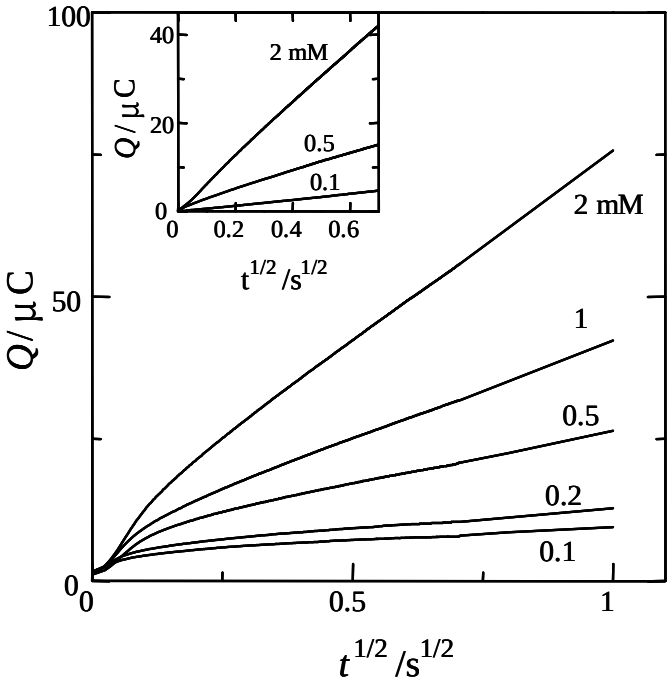

Fig. 12

Takahiro YAMAGUCHI*, Teruhisa KOMURA, Sayomi HAYASHI, Manabu ASANO, Guang Yao NIU, Kohshin TAKAHASHI

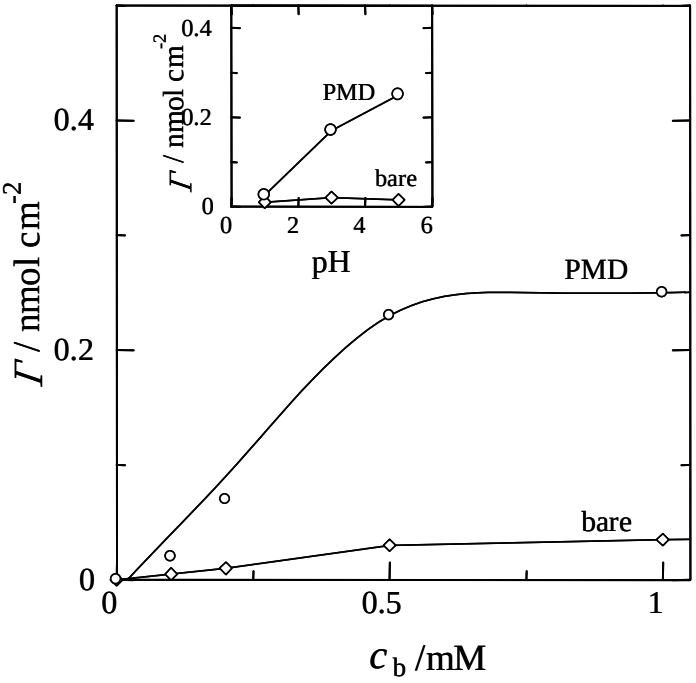

Fig. 13

Takahiro YAMAGUCHI*, Teruhisa KOMURA, Sayomi HAYASHI, Manabu ASANO, Guang Yao NIU, Kohshin TAKAHASHI